Journal of Applied Mechanics and Technical Physics, Vol. 48, No. 1, pp. 34–43, 2007

NUMERICAL AND EXPERIMENTAL STUDY OF THE FINE STRUCTURE OF A STRATIFIED FLUID FLOW OVER A CIRCULAR CYLINDER

V. A. Gushchin,[1] **V. V. Mitkin,**[2]
T. I. Rozhdestvenskaya,[1] **and Yu. D. Chashechkin**[2]

UDC 551.555.9

The fine structure of the flow field of a continuously stratified fluid around a circular cylinder for small values of the Froude number was investigated in laboratory and numerical experiments. The parameters of the leading perturbation, the internal-wave field, and the cylinder wake were calculated using a two-dimensional model. The existence of the previously experimentally observed high-gradient density layers in the wake that are parallel to the flow axis was for the first time confirmed by numerical calculations. Results of the numerical and experimental studies are in good agreement with each other and with analytical models for small values of the Froude number.

Key words: *stratified fluid, circular cylinder, internal-wave field, wake, fine structure, computational experiment.*

Introduction. The space–time characteristics of continuously stratified fluid flows over two-dimensional obstacles, their stability, and critical restructuring conditions are of scientific and practical interest because in nature and in technological devices, fluids are stratified due to nonuniform distributions of temperature and concentration of dissolved or suspended materials.

In an analysis of stratified fluid flows taking into account stratification, the equations of hydrodynamics are supplemented by a buoyancy force and the diffusion equation for the stratifying component. As a result, along with a boundary layer, a trailing wake, bottom vortices, and a vortex trail, the flow structure contains internal waves and a leading perturbation. It should be noted that a stratified fluid is a nonequilibrium medium, in which even in the absence of external destabilizing factors, boundary flows with individual velocity and density scales are formed on impermeable surfaces because of the interruption of the flow of the stratifying component [1]. In this case, the solution of the problem is considerably complicated by the occurrence of new small and large parameters due to the weakness of the stratification and the smallness of the terms due to diffusion.

The most widely used stratification models are the two-layer fluid model, for which calculations are performed by analogy with surface waves, and the exponentially stratified model. Because of the weak stratification in the formulation of the problem, the Navier–Stokes equation are written in the Boussinesq approximation, in which the density changes are considered negligibly small in all terms of the equation, except in the term containing gravity that takes into account buoyancy.

There have been extensive experimental studies of linearly stratified fluid flows around a horizontal cylinder (exponential and linear density distributions are indistinguishable within the experimental error in the case of weak stratification). In most of these studies, the flow structure was visualized by optical methods and geometrical characteristics of waves, vortices, and wakes were determined. The phenomenological classification of flow regimes [2] was extended and supplemented in [3] taking into account high-gradient layers in wakes. New types of instability of laminar flow past a cylinder at low Froude number were found in [4].

[1]Institute of Computer Aided Design, Russian Academy of Sciences, Moscow 123056; gushchin@icad.org.ru.
[2]Institute of Problems of Mechanics, Russian Academy of Sciences, Moscow 117526; chakin@ipmnet.ru. Translated from Prikladnaya Mekhanika i Tekhnicheskaya Fizika, Vol. 48, No. 1, pp. 43–54, January–February, 2007. Original article submitted October 17, 2005; revision submitted February 26, 2006.

Analytical calculations of leading perturbations use the assumption that the fluid is ideal and that all perturbations damp at large distances ahead of the obstacle [5]. Aksenov et al. [6] examined the range of applicability of this approach to the analysis of the main features of flow around a cylinder: blocked fluid ahead of the obstacle, attached internal waves, hanging vortex systems (rotors by the terminology of [6]). Although formally the method of [5] applies to flow calculations for large values of the Froude number $\mathrm{Fr} = U/ND > 0.5$ (U is the velocity of the cylinder; D is the diameter of the cylinder; and N is the buoyancy frequency), it is also appropriate at low Froude number.

In the numerical modeling of stratified flows, extensive use has been made of the splitting method, which was originally proposed for the calculation of homogeneous fluid flows [7]. A detailed description of this method and various examples of its use for two- and three-dimensional nonstationary stratified fluid flows, including free-surface flows, are given in [8, 9]. Results of calculations and experimental studies of attached internal waves past a cylinder are in good agreement [10]. Although the method of splitting in physical parameters has large potential, it has previously been employed primarily to calculate large-scale elements of wakes and attached internal waves. The fine structure elements of stratified flows underlying the phenomenological classification of flow regimes has not been analyzed previously. The advent of new powerful computers allows a better use of the potential of computational approaches and detailed flow calculations.

The purpose of the present work was to adapt the splitting method [7] (which has been successfully used to analyze homogeneous fluid flows) to the calculation of the structure of two-dimensional stratified flows, to compare results of computational and laboratory experiments for the same values of the dimensionless parameters of the problem, and to analyze the transverse flow pattern past a cylinder.

1. Formulation of the Problem. We consider transverse flow of a linearly stratified fluid around a cylinder of diameter D; the fluid density $\rho(y) = \rho_0(1 - y/\Lambda + s)$ decreases with increasing height y due to a change in salinity [$\rho_0 = \rho(0) = 1$, Λ is the stratification scale, and s is the salinity perturbation]. This phenomenon is described by the system of equations that includes the Navier–Stokes equations written in the Boussinesq approximation, which is applicable due to the weak stratification, the fluid compressibility equation, and the salt diffusion equation:

$$\frac{\partial \boldsymbol{v}}{\partial t} + (\boldsymbol{v}\nabla)\boldsymbol{v} = -\frac{\nabla p}{\rho_0} + \boldsymbol{g}s + \nu\nabla^2\boldsymbol{v},$$

$$\operatorname{div}\boldsymbol{v} = 0, \tag{1}$$

$$\frac{\partial s}{\partial t} + (\boldsymbol{v}\nabla)s = \varkappa_s\nabla^2 s + \frac{1}{\Lambda}\,v_y.$$

Here $\boldsymbol{v}$ is the velocity, p is the pressure, $\boldsymbol{g}$ is the acceleration of gravity, ν is the kinematic viscosity, and $\varkappa_s$ is the salt diffusion coefficient. Stratification is characterized by the linear scale $\Lambda = |d(\ln\rho)/dy|^{-1}$ and the buoyancy period $T_b = 2\pi/N = 2\pi\sqrt{\Lambda/g}$ [11]. The flow velocity at infinity is equal to U. In the calculations and experiments, the fluid with a buoyancy period $T_b = 25.2$ was studied.

The boundary conditions include unperturbed flow conditions on the contour G at a large distance from the center: $u = U\cos\theta$, $v = -U\sin\theta$, $p = 0$, and $s = 0$; the attachment condition $\boldsymbol{v}|_\Gamma = 0$, and the condition of the absence of the normal component of the salinity flux $\partial s/\partial n|_\Gamma = 0$ on the surface of the cylinder Γ [u and v are the velocity components along the polar coordinate (r, θ)].

The initial condition for the velocity is the unperturbed plane-parallel flow $u = U\cos\theta$, $v = -U\sin\theta$ taking into account the boundary conditions on the cylinder surface.

The basic scales of the problem (in addition to the external scales — the body size and the buoyancy scale) are the dimensions of the structural elements of the flow: the length of the attached internal wave $\lambda = UT_b = 2\pi U/N$, the thickness of the velocity boundary layer $\delta_u = \nu/U$, and the thickness of the density boundary layer $\delta_\rho = \varkappa_s/U$. The scale of the internal boundary flow due to stratification is $\delta_N = \sqrt{\nu/N}$, the scale of the corresponding density inhomogeneity is equal to $\delta_s = \sqrt{\varkappa_s/N}$ [2].

The ratios of the basic scales form the main dimensionless parameters: the Reynolds number $\mathrm{Re} = D/\delta_u = UD/\nu$, the Peclet number $\mathrm{Pe} = D/\delta_\rho = UD/\varkappa_s$ (or the Schmidt number $\mathrm{Sc} = \mathrm{Pe}\,/\,\mathrm{Re}$), and the internal Froude number $-\mathrm{Fr} = \lambda/(2\pi D) = U/(ND)$; the scale ratio is $C = \Lambda/D$. Since the stratification is weak and the kinetic coefficients are small, the values of the basic scales differ significantly: $\Lambda \gg D \gg \delta_u \gg \delta_\rho$, $\lambda \gg \delta_\nu \gg \delta_s$. The technique of the laboratory experiment and the computational approaches were developed taking into account the necessity of distinguishing structural elements with different scales.

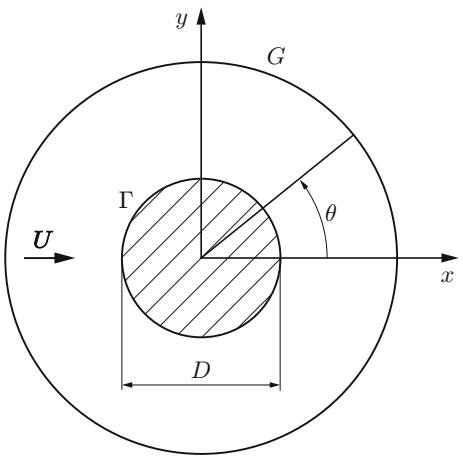

Fig. 1. Computational flow domain.

For the flow velocity U as the velocity scale and the cylinder diameter D as the length scale, system (1) is written in dimensionless form as follows:

$$\frac{\partial \boldsymbol{v}}{\partial t} + (\boldsymbol{v}\nabla)\boldsymbol{v} = -\frac{\nabla p}{\rho_0} + \frac{s\boldsymbol{g}}{\mathrm{Fr}^2\,|g|(D/\Lambda)} + \frac{1}{\mathrm{Re}}\,\nabla^2\boldsymbol{v},$$

$$\operatorname{div}\boldsymbol{v} = 0, \tag{2}$$

$$\frac{\partial s}{\partial t} + (\boldsymbol{v}\nabla)s = \frac{1}{\mathrm{Pe}}\,\nabla^2 s + \frac{Dv_y}{\Lambda}.$$

The computational domain is enclosed between two concentric circles — the boundary of the cylinder Γ and the conditional boundary G behind which there is the unperturbed region (Fig. 1). The fluid flow moving around the motionless cylinder at velocity U is directed along the x axis (in the experiment, the cylinder moves in a motionless fluid). The calculations are performed using polar coordinates (r, θ) with origin at the center of the cylinder. The outer boundary is at a distance $(80\text{–}100)D$, depending on the conditions of the problem.

2. Computational Procedure. For convenience, the computational domain is transformed to a rectangular region with sides z in the horizontal direction and θ in the vertical direction by means of the substitution $r = R(z) = 1 + \alpha z + z^3$ with the transformation coefficient $\alpha = 0.2\sqrt{2/\mathrm{Re}}$. The new orthogonal coordinate system (z, θ), where $z \in [0, \infty]$ and $\theta \in [0, 2\pi]$, is related to the Cartesian system by the transformation $x = R(z)\cos\theta$, $y = R(z)\sin\theta$. The computational grid in the coordinates z and θ is uniform and is more convenient than polar grids in using finite-difference methods. At the same time, this grid provides a better resolution of flow singularities near the cylinder.

System (2) is solved using the method of splitting in physical variables with an explicit hybrid finite-difference scheme of the second-order approximation in spatial variables. This scheme is characterized by monotony and minimum scheme viscosity and dispersion, which allows calculations to be performed over a wide range of values of the Reynolds and Froude numbers [7]. In the splitting method, problem (2) is solved stage by stage. At a certain time $t_n = n\Delta\tau$ ($\Delta\tau$ is the time step and n is the number of steps), let the velocity field $\boldsymbol{v}^n$ be known. Then, the scheme of determining the unknown functions at the time $t_{n+1} = (n+1)\Delta\tau$ can be represented as follows. In the first stage, we determine an auxiliary grid function $\tilde{\boldsymbol{v}}$ that takes into account only convective and viscous terms and buoyancy forces but ignores the condition $\operatorname{div}\boldsymbol{v} = 0$:

$$\frac{\tilde{\boldsymbol{v}} - \boldsymbol{v}^n}{\Delta t} = -(\boldsymbol{v}^n\nabla)\boldsymbol{v}^n + \frac{1}{\mathrm{Re}}\,\nabla^2\boldsymbol{v}^n + \frac{s\boldsymbol{g}}{\mathrm{Fr}^2\,|g|(D/\Lambda)}.$$

In the second stage, the pressure field is found from the solution of the Poisson equation taking into account the condition $\nabla\boldsymbol{v}^{n+1} = 0$:

$$\nabla^2 p = \frac{\nabla\tilde{\boldsymbol{v}}^n}{\Delta t}.$$

In the third stage, we calculate the velocity field in the $(n+1)$th time layer:

$$\boldsymbol{v}^{n+1} = \tilde{\boldsymbol{v}} - \nabla p\, \Delta t,$$

after which, using the obtained value of $\boldsymbol{v}^{n+1}$, we solve the equation for the salinity perturbation

$$s^{n+1} = s^n - \Delta t(\boldsymbol{v}^{n+1}\nabla)s - \frac{\Delta t\, \Delta s}{\mathrm{Pe}} + \frac{\Delta t\, D(u\sin\theta + v\cos\theta)}{\Lambda}.$$

The calculations were carried out until the time $10T_b = 252$, to which the results of the experiments corresponded. The computational grid contained 180 points on the coordinate z and 180 points on the coordinate θ (the sizes of the first cell 0.07×0.044 cm are sufficient to resolve the fine structure of the flow). The time step was chosen automatically from the Courant condition. The calculations were performed on a PARAM-10000 supercomputer (Ultra Sparc II, 400 MHz). All numerical data presented for comparison with the experimental results were converted to the Cartesian coordinates in which the cylinder moves relative to the motionless fluid.

3. Experimental Technique. The experiments were carried out in a $240\times40\times60$ cm tank with transparent walls. The tank was filled with a linearly stratified aqueous solution of table salt using the method of continuous displacement. Before each experiment, we measured the density distribution and the buoyancy period by records of the oscillations induced by a density marker and recorded by an electrical conductivity probe (the error did not exceed 5%). In this series of experiments, the buoyancy period was $T_b = 25.2$ sec.

We studied the flow pattern past a horizontal cylinder of diameter $D = 2.5$ cm which was towed at a constant velocity in the center of the tank. The cylinder was fastened with thin knifes to a carriage, which moved in guides at a velocity $U = 0.08$–3.00 cm/sec (step $\Delta U = 0.02$ cm/sec; the error in determining the velocity was not more than 5%). The conditions of the experiments ($C = 150$–560, $\mathrm{Fr} = 0.12$–0.73, and $\mathrm{Re} = 20$–75) corresponded to a laminar wake. Before the beginning of each experiment, the cylinder was placed near the end wall of the tank.

Visualization was performed with an IAB-458 shadow device using the Maksutov method in two modifications: "vertical slit–knife" or "slit–filament in focus." In view of the linear relation between the density and refraction coefficient of the salt solution, the horizontal component of the refraction coefficient is visualized in the first method and its modulus in the second method. Density markers were produced by vertically rising gas bubbles or falling sugar crystals. The characteristic life time of a marker was 40–100 sec, and its thickness was not more than 1 mm. The error in measuring the fluid velocity did not exceed 10%.

The buoyancy period, salinity profiles, and salinity variation at a chosen point were measured by a single-electrode contact specific-conductivity probe. The probe was calibrated before each series of experiments directly in the laboratory tank using the methods of lift-and-drop to a height of 0.5 cm and sweep-vibrations. The static and dynamic errors of the measurements were 15%.

In 24 h after the tank with the cylinder installed under the carriage was filled, when all perturbations decayed and the density distribution became uniform, we measured the salinity profile and the buoyancy period on the chosen horizon. Then, vertical markers — flow profile markers — were created in the tank and the cylinder was towed over the entire length of the tank. The next experiment was performed after the damping of all motions and the salinity (density) perturbations from the previous towage.

4. Main Results. For comparison with the experiment with an aqueous solution of table salt (NaCl), the calculations were performed for the following parameter values: $\nu = 0.01$ cm^2/sec, $\varkappa_s = 1.41\cdot10^{-5}$ cm^2/sec, $T_b = 25.2$ sec, $U = 0.1$–0.4 cm/sec, and $D = 2.5$ cm.

A typical shadow pattern of the laminar stratified flow around the cylinder and the calculated map of salinity isolines in a coordinates system attached to the cylinder are given in Fig. 2 (the cylinder moves from right to left). In the shadow pattern, which is obtained by the "vertical slit–filament in focus" method, one can see the structure of the field of the salinity gradient modulus (Fig. 2a). The markers visualize the velocity profiles in the leading perturbation and in the cylinder wake. Figure 2b gives the salinity perturbation field.

In Fig. 2, one can also see the common elements of the observed and calculated patterns: the leading perturbation, the velocity and density wakes past the cylinder, and the internal-wave field. The leading perturbation consists of the blocked fluid immediately in front of the body and nonstationary internal waves, which smoothly become attached internal waves behind the cylinder. In both the shadow and calculated patterns, one can see the wedge-shaped boundaries of the region of complete blocking in front of the cylinder.

The distorted semi-circles behind the cylinder in Fig. 2a visualize the phase surfaces of the attached internal waves. Dark lines correspond to crests, and gray lines to troughs. The crests and troughs of the attached waves are

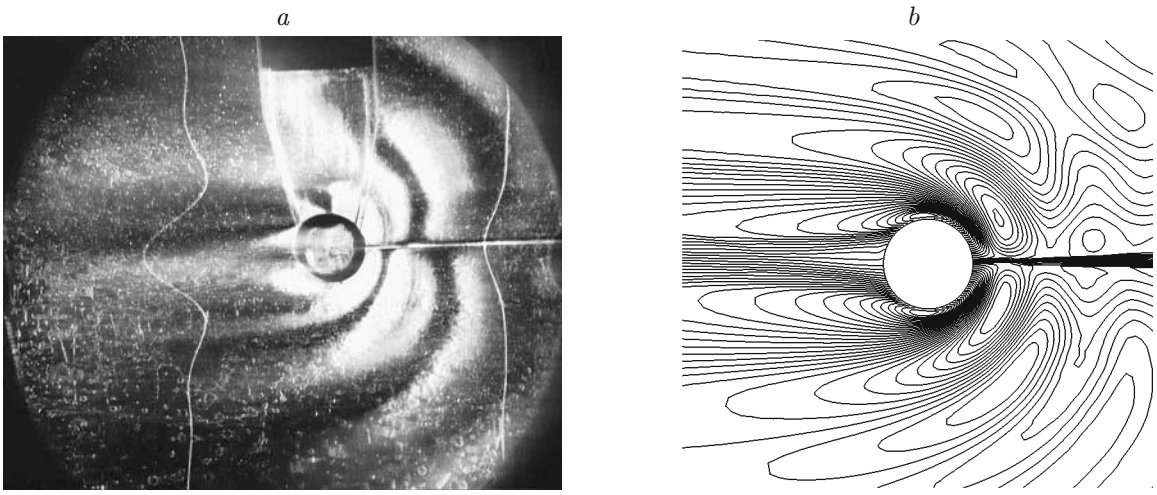

Fig. 2. Stratified flow around the cylinder ($D = 2.5$ cm, $U = 0.1$ cm/sec, $T_b = 25.2$ sec, Fr $= 0.16$, and Re $= 25$): (a) shadow pattern; (b) calculated salinity isolines.

also clearly evident in the salinity isoline pattern (Fig. 2b). In both cases, three waves are visualized, whose length agrees with that calculated by linear theory: $\lambda = U_0 T_b$ [5]. However, the calculated pattern is more informative since it allows one to determine not only the shape of the wave crests and troughs but also the salinity perturbation magnitude, and hence, the particle displacement in the wave and the position of the regions of the maximum amplitudes (the centers of the closed isolines).

In both the calculations and the experiment, the phase surfaces of the attached internal waves deviate from semi-circles in the vicinity of the density wake, where they are entrained in the middle flow due to the Doppler effect. The largest density perturbations are observed near the axis of motion in the leading perturbation and immediately behind the cylinder. Generally, the experimentally observed and calculated flow patterns are structurally similar. More detailed results of experimental studies of blocked-fluid parameters ahead of a two-dimensional obstacle are given in [12].

The salinity perturbation field has a different structure. The family of almost parallel isolines in front of the cylinder indicates the presence of blocking (pushing of the fluid ahead of the body). The inclined lines which gradually become concentric circles visualize nonstationary leading internal waves (to which the inclined half-lines in Fig. 2a correspond), which smoothly become attached waves behind the body. However, near the flow axis in the wake past the body, the density variation ceases to be monotonic. In the bottom region, a central high-gradient envelope (the condensation of isolines in Fig. 2b and light band behind the body in Fig. 2a) adjoins the obstacle. Previously, high-gradient elements of wake structures have been observed in experiments but not visualized in numerical calculations.

The occurrence of an interior layer in the wake is due to the general restructuring of the stratification by the moving cylinder. Because of the blocking, i.e., deceleration and entrainment of the fluid, a more homogeneous fluid collected from the body trajectory is accumulated in front of the two-dimensional cylinder. The entrained fluid is replaced by a new fluid, which is supplied from the fluid layers previously separated vertically and is submerged under the action of buoyancy forces. In the regions of contact of the fluid of different density behind the cylinder, one or several high-gradient layers are formed, depending on motion parameters. Low Froude numbers flows are classified according to the number and position of density discontinuity surfaces in the wake [12]. Previously, the high-gradient layers observed in flows over two-dimensional and three-dimensional obstacles have not been found in numerical calculations.

The density perturbation profiles behind the cylinder calculated at various distances from its rear critical point are given in Fig. 3. Salinity perturbations are plotted on the additional axis. Point 0 corresponds to the center of the two-dimensional cylinder. In each section on the axis of motion there is a thin layer in which the density gradient is several orders of magnitude larger than the background density gradient. In the section the nearest to

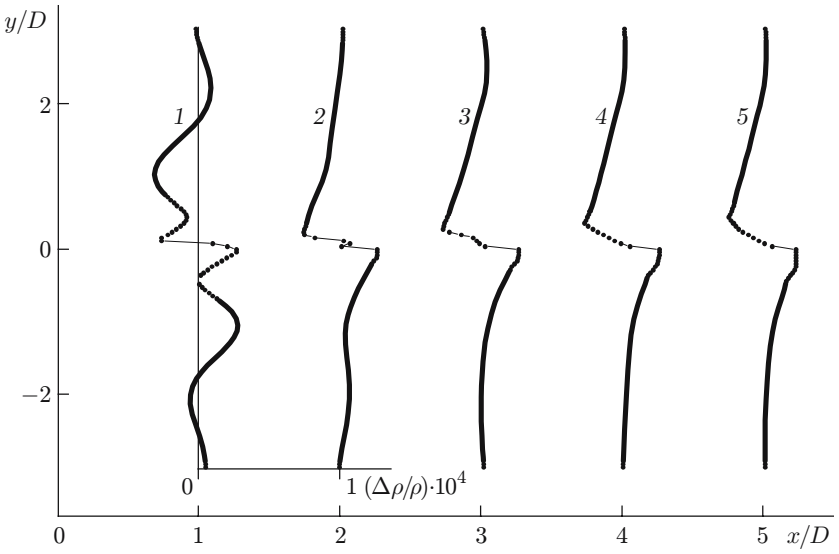

Fig. 3. Density profiles in the wake past the cylinder at various distances from the rear critical point ($D = 2.5$ cm, $U = 0.1$ cm/sec, $T_b = 25.2$ sec, Fr = 0.16, and Re = 25): $x/D = 1$ (1), 2 (2), 3 (3), 4 (4), and 5 (5).

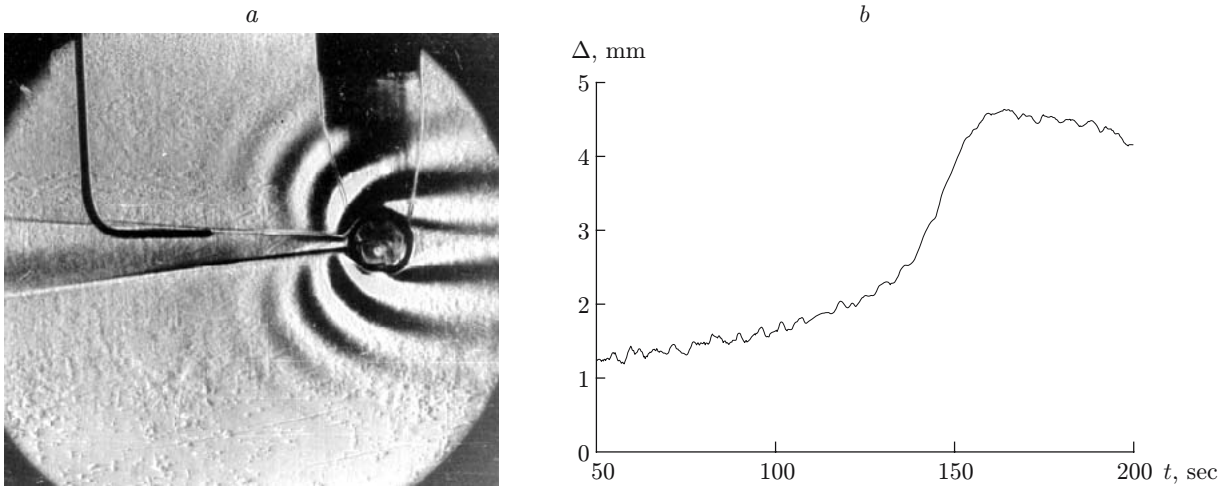

Fig. 4. Visualization of layers on the wake boundary (a) and measured density variations during the flow formation behind the cylinder (b) ($D = 2.5$ cm, $U = 0.1$ cm/sec, $T_b = 25.2$ sec, Fr = 0.16, and Re = 25).

the cylinder, a density jump is formed because of the merging of the layers separated vertically in the unperturbed medium.

In the given density distributions, the wave perturbations are manifested only in the section the nearest to the body, at a distance from the rear critical point of the cylinder equal to the wavelength, which is indicative of the influence of the waves the nearest to the cylinder (see Fig. 2). With distance from the cylinder, the density jump is gradually smoothed out because of diffusion. On the axis of motion in the vertical sections the nearest to the cylinder, the magnitude of the density jump obtained by calculations (see Fig. 3) corresponds to the merging of the unperturbed-fluid layers separated vertically by a distance $h \approx 0.7$ cm. This results agrees with measurements of density variations on the high-gradient envelope of the wake.

The measurements were performed in the initial stage of flow formation, in which the envelope of the density wake past the obstacle is split (Fig. 4a). During the flow formation, the envelopes move toward each other at an almost constant velocity. After they merge, a central layer is formed on the axis of motion in the density wake. The slow uniform motion of the envelopes during the flow formation allows the magnitude of the density jump to be measured directly by the single-electrode electrical-conductivity probe with higher accuracy than in the ordinary probing, because of the absence of electrical noise and additional vibrations.

The spatial resolution of the probe is 2.5 mm, which exceeds the thickness of the layer. However, the high sensitivity of the probe allows one to estimate the thickness and density change. For this purpose, the probe was installed on the carriage and moved together with the cylinder at a fixed distance from it. During the flow formation, the merging inclined envelopes of the wake form a wedge-shaped region behind the cylinder (Fig. 4a). As the cylinder moves from left to right, the inclined layer moving from top to bottom crosses the probe placed at the fixed horizon.

In such measurements, the static and dynamic graduation of the probe is performed immediately before the experiment by the method of lift-and-drop to a height of 0.5–1.0 cm. The graduation results make it possible to directly determine the deviation of the fluid layers from the initial level in the initial density field (the parameter Δ). A record of the electrical conductivity probe is given in Fig. 4b.

The time variation in the output signal of the electrical conductivity probe indicates that the density field undergoes restructuring over the entire tank simultaneously with the beginning of motion of the cylinder. By the moment the cylinder appeared in the field of the shadow device ($t = 50$), the displacement of the fluid particles reaches $\Delta = 1.4$ mm, indicating a decrease in the density on the horizon of the probe location. Slow growth in the signal is replaced by a rapid change at $t = 150$ sec. Figure 4a corresponds to exactly this time (the moment the wake envelope crosses the working volume of the probe). Since the scale of resolution of the probe is much larger than the shell thickness, the probe output signal smooths out. Nevertheless, the displacements of the layers determined by the above-mentioned method are 2–3 mm, which agrees with the calculation results given in Fig. 3. In this case, the density gradient in the envelope increases severalfold (depending on motion parameters) in comparison with the background density gradient [12]. During the motion of the cylinder, the density profiles behind the body smooth out gradually because of diffusion, which corresponds to the reduction in the contrast of the envelope images in the shadow patterns (see Fig. 4a) and is supported by direct measurements of electrical conductivity. Next, the probe output signal begins to decrease gradually, indicating recovery of the initial density distribution after the passage of the cylinder.

The results of measurements and numerical and analytical calculations of velocity profiles in front of the cylinder are presented in Fig. 5. Vertical velocity profiles are plotted on the additional axis. The analytical calculations of the perturbations of the horizontal velocity components u were performed using the results of [5]. Converting the expressions obtained in [5], we write the horizontal velocity as

$$\frac{u}{Uk_0^2D^2} = -2\pi\,\frac{Y_1(k_0r)}{k_0r}\,\cos 2\theta - 2\pi Y_0(k_0r)\sin^2\theta$$

$$+\,8\sum_{n=0}^{\infty}\frac{4n^2+4n-1}{(4n^2-1)\,(2n+3)}\,J_{2n+1}(k_0r)\,\cos(2n+1)\theta. \qquad (3)$$

Here r and θ are the radius-vector and the polar angle in the cylindrical coordinate system attached to the cylinder, $k_0 = N/U$, and $Y_n(k_0r)$ and $J_n(k_0r)$ are Neumann and Bessel cylindrical functions, respectively. Expression (3) is significantly simplified on the axis of motion, where $\theta = 0$ and the trigonometric functions vanish:

$$\frac{u}{Uk_0^2D^2} = \frac{2\pi}{k_0|x|}\,[H_1(k_0|x|)\,\mathrm{sgn}\,x - Y_1(k_0|x|)]. \qquad (4)$$

Here $H_1(k_0|x|)$ is the complete Struve function and $Y_1(k_0|x|)$ is a first-order Neumann function.

At the center of the blocked-fluid region, the velocity perturbations decay monotonically with distance from the body. This leads to variation in the position of the zero streamline, on which the fluid and body velocities are equal, i.e., in fact, there is deformation of the cylinder contour in the flow [6].

The position of the extreme point of the intersection of the contour of the completely blocked fluid and the line of the center of the wake in front of the cylinder agrees with the parameters of the experimentally observed

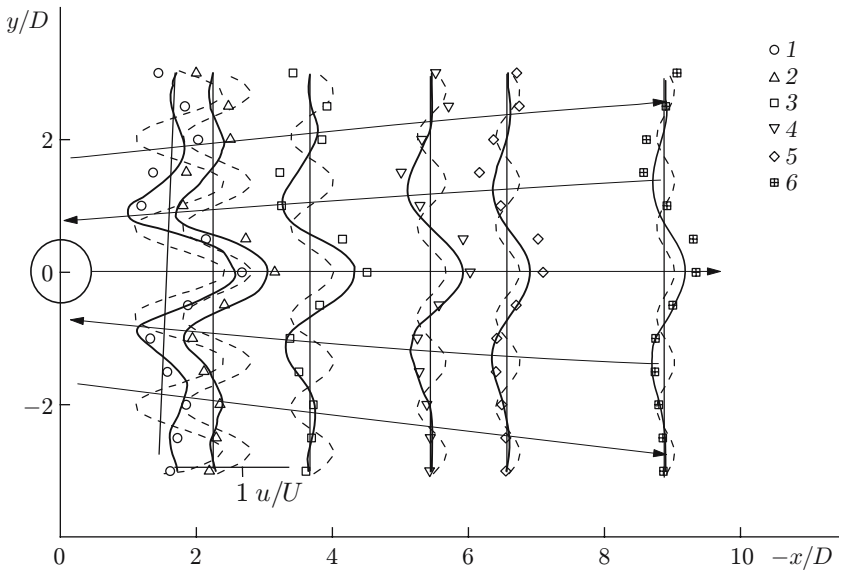

Fig. 5. Velocity profile in front of the cylinder in various vertical sections ($D = 2.5$ cm, $U = 0.135$ cm/sec, $T_b = 25.2$ sec, Fr = 0.22, and Re = 33.8): the solid curves refer to experimental data and the dashed curves to calculations using formula (5.1); the points are results of numerical calculation for $x/D = 1.75$ (1), 2.3 (2), 3.7 (3), 5.5 (4), 6.6 (5), and 8.9 (6); the arrows show the fluid velocity direction.

blocking of the fluid during slow motion of the cylinder. Irrespective of the shape of the obstacle, the velocity profile in the leading perturbation has a wavy structure and is symmetric about the central horizontal plane [4], which agrees qualitatively with the calculation results (see Fig. 2). The main maximum of the perturbation is on the axis of motion, where the direction of the fluid velocity coincides with the direction of motion of the cylinder. Above and below the regions of the blocked fluid and the wake, there are jets with alternating velocity directions. Near the body, the vertical distance between the first zero values of the velocity is approximately equal to the height of the cylinder.

The distance between the centers of the jets adjoining the blocking region exceeds the height of the cylinder and increases with distance from the body, which is inconsistent with the ideal fluid models, which ignore the real cylinder shape [5]. In addition, the position of the lines of the jet maxima and minima is determined by the flow regime. The distances between the unidirectional jets in the upper and lower half-spaces for the given section increase with increasing Froude number in proportion to the length of the attached internal wave. The results on the amplitude and phase do not agree with experimental data. In this case, the difference in the phase patterns is due to the fact that the dipole model ignores the dimensions of the cylinder and the position of the jets is determined only by the length of the attached internal wave. From the calculation results [6], it follows that a decrease in the Froude number leads to a large deformation of the contour of the zero stream function, which in fact defines the cylinder shape when a real body is replaced by a mass dipole. Formula (4) implies that as the Froude number decreases, the streamline contour is highly stretched in the direction of motion of the body and its frontal point recedes from the source. In this case, the streamline contour is compressed and its height becomes smaller than the height of the streamline cylinder.

For small values of the Froude number, a nearly planar segment similar in dimension to the cylinder diameter is observed on the experimental profile of the horizontal velocity component near the axis of motion in front of the cylinder, i.e., in experiments with bodies of large dimension ($D > \lambda$), nonstationary internal waves do not penetrate into the region of complete flow blocking, which agrees with the data of [12].

The numerical calculation provides high-accuracy predictions of the phase structure of the velocity field in front of the cylinder and the positions of the lines of minima and maxima; the calculated and measured velocity values almost coincide (see Fig. 5). The slight difference in the velocity values calculated and measured on the peripheral jets is due to the smallness of the velocity perturbations in this region, which increases the measurement error.

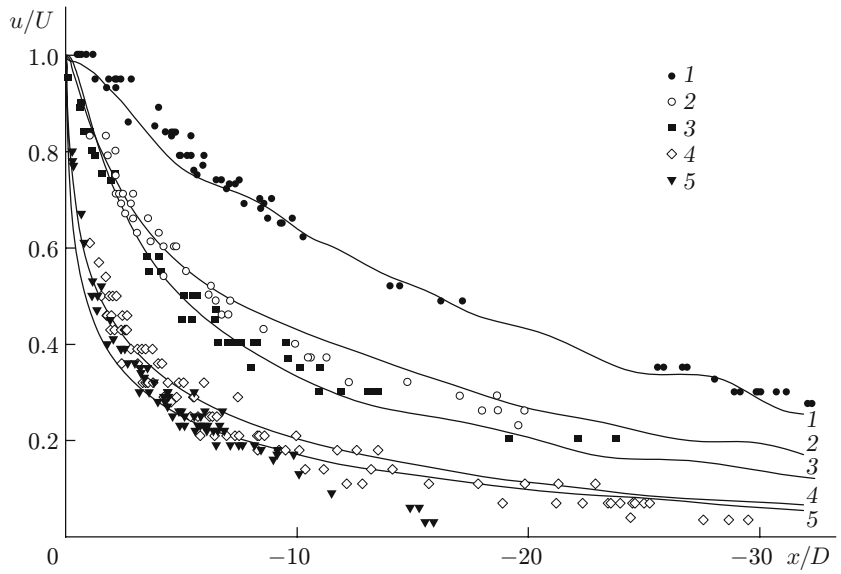

Fig. 6. Calculated (solid curves) and measured (points) velocity perturbation distributions on the axis of motion in front of the cylinder ($D = 2.5$ cm and $T_b = 25.2$ sec): 1) $U = 0.1$ cm/sec, Fr = 16, and Re = 25; 2) $U = 0.17$ cm/sec, Fr = 0.27, and Re = 43; 3) $U = 0.21$ cm/sec, Fr = 0.34, and Re = 53; 4) $U = 0.28$ cm/sec, Fr = 0.46, and Re = 71; 5) $U = 0.4$ cm/sec, Fr = 0.64, and Re = 101.

Calculated and measured velocity distributions on the axes of motion in front of the cylinder versus distance to the frontal critical point of the cylinder are presented in Fig. 6. In both the numerical calculations and experiments, the velocity perturbation decreases monotonically with distance from the body. In the slowest regimes, a blocking region occurs in the immediate proximity of the cylinder. The measured and calculated velocity perturbations are in good agreement. The nonmonotonic nature and oscillations of the velocity in the leading perturbation for low velocities of motion of the cylinder are due to the effect of flow reflection from the end wall of the tank. In the numerical calculations, oscillations are a consequence of the boundary condition imposed on the outer contour of the computation domain.

Conclusions. The results of flow visualization and velocity measurements for the uniform motion of a horizontal cylinder in a continuously stratified fluid are in fair agreement with the results of numerical calculations. In the computational and laboratory experiments, the blocked fluid in front of the cylinder is surrounded by a field of nonstationary waves whose phase surfaces are located on inclined half-lines. In the analytical models that use insufficiently rigorous additional assumptions (Boussinesq approximation, neglect of the singular components of solutions due to viscosity and (or) diffusion, simplified boundary conditions), the phase surfaces in the leading perturbation are arranged horizontally. The high-gradient layers in the cylinder wake observed in experiments for arbitrary (in particular, minimal) values of the Froude number were revealed for the first time in the computational experiment.

This work was supported by the Russian Foundation for Basic Research (Grant Nos. 05-01-00496 and 02-05-65383), the Foundation for Domestic Science Support and the Presidium of the Russian Academy of Sciences (6th assessment competition, grant No. 94 “Formation and Evolution of Free Stratified Flows”), and the Program of the Presidium of the Russian Academy of Sciences “Mathematical Modeling.”

REFERENCES

1. V. G. Baidulov, and Yu. D. Chashechkin, “Effect of diffusion on the boundary flows in a continuously stratified fluid,” *Izv. Ross. Akad. Nauk, Fiz. Atmos. Okeana*, **29**, No. 5, 666–672 (1993).
2. D. L. Boyer, P. A. Davies, H. J. S. Fernando, and X. Zhang, “Linearly stratified flow past a horizontal circular cylinder,” *Philos. Trans. Roy. Soc. London, Ser. A*, **328**, 501–528 (1989).

3. Yu. D. Chashechkin and I. V. Voeikov, "Vortex systems past a cylinder in a continuously stratified fluid," *Izv. Ross. Akad. Nauk, Fiz. Atmos. Okeana*, **29**, No. 6, 821–830 (1993).
4. V. V. Mitkin amd Yu. D. Chashechkin, "Structure of stratified flow around a cylinder at low internal Froude number," *J. Appl. Mech. Tech. Phys.*, **40**, No. 1, 69–75 (1999).
5. R. R. Long, "Some aspects of the flow of stratified fluids. 1. A theoretical investigation," *Tellus*, **5**, No. 1, 42–58 (1953).
6. A. V. Aksenov, V. A. Gorodtsov, and I. V. Sturova, "Modeling stratified ideal incompressible fluid flow around a cylinder," Preprint No. 282, Institute of Problems of Mechanics, USSR Academy of Sciences (1986).
7. V. A. Gushchin, "Splitting method for the problems of dynamics of an inhomogeneous viscous incompressible fluid," *Zh. Vychsil. Mat. Mat Fiz.*, **21**, No. 4, 1003–1017 (1981).
8. O. M. Belotserkovskii, *Numerical Modeling in Continuum Mechanics* [in Russian], Nauka, Moscow (1984).
9. O. M. Belotserkovskii, V. A. Gushchin, and V. N. Kon'shin, "Splitting method for investigating stratified fluid flows with a free surface," *Zh. Vychsil. Mat. Mat. Fiz.*, **27**, No. 4, 594–609 (1987).
10. O. M. Belotserkovskii, S. O. Belotserkovskii, V. A. Gushchin, et al., "Numerical and experimental modeling of gravitational internal waves during motion of a body in a stratified fluid," *Dokl. Akad. Nauk SSSR*, **279**, No. 3, 562–566 (1984).
11. V. G. Baidulov and Yu. D. Chashechkin, "Flow formation at the beginning of motion of a horizontal cylinder in a continuously stratified fluid," *Izv. Ross. Akad. Nauk, Fiz. Atmos. Okeana*, **35**, No. 6, 821–828 (1999).
12. V. V. Mitkin, "Experimental study of the velocity field ahead of a two-dimensional obstacle in a continuously stratified fluid," *Izv. Ross. Akad. Nauk, Fiz. Atmos. Okeana*, **37**, No. 1, 85–92 (2001).